Nature of the apical and planar oxygen bonds in the $Sr_{n+1}Ru_nO_{3n+1}$ family ($n = 1,2,3$)

M. Malvestuto,[1,2,*] V. Capogrosso,[1,2] E. Carleschi,[3] L. Galli,[4,5] E. Gorelov,[6] E. Pavarini,[6,7] R. Fittipaldi,[8,9] F. Forte,[8,9] M. Cuoco,[8,9] A. Vecchione,[8,9] and F. Parmigiani[1,2]

[1]*Elettra-Sincrotrone Trieste, S.S. 14 km 163.5, Area Science Park, I-34149 Basovizza (Ts), Italy*
[2]*Department of Physics, University of Trieste, via A. Valerio 2, I-34127, Trieste, Italy*
[3]*Department of Physics, University of Johannesburg, PO Box 524, Auckland Park 2006, South Africa*
[4]*Center for Free-Electron Laser Science (CFEL), DESY, Notkestrasse 85, D-22607 Hamburg, Germany*
[5]*Department of Physics, University of Hamburg, Luruper Chaussee 149, D-22761 Hamburg, Germany*
[6]*Institute for Advanced Simulation, Forschungszentrum Jülich, D-52425 Jülich, Germany*
[7]*JARA High-Performance Computing, RWTH Aachen, D-Aachen, Germany*
[8]*CNR-SPIN Salerno, Via Giovanni Paolo II, I-84084 Fisciano (SA), Italy*
[9]*Department of Physics, University of Salerno, Via Giovanni Paolo II, I-84084 Fisciano (SA), Italy*

(Received 8 August 2013; revised manuscript received 31 October 2013; published 22 November 2013)

We investigate the electronic structure of the $Sr_{n+1}Ru_nO_{3n+1}$ family ($n = 1,2,3$) in the vicinity the Fermi level by means of polarization-dependent resonant O 1*s* x-ray emission spectroscopy. Using both energy window and polarization analysis we disentangle the contribution of apical and planar oxygen, and compare it with first-principles calculations. Our results provide a new insight on the nature of the oxygen bonds and the role of Sr 3*d* states.

DOI: 10.1103/PhysRevB.88.195143 PACS number(s): 78.70.Dm, 78.70.En, 74.70.Pq, 71.20.Be

I. INTRODUCTION

Metallic Ruddlesden-Popper $Sr_{n+1}Ru_nO_{3n+1}$ ruthenates (in short SRO) with 2/3 filled 4*d* t_{2g} bands have emerged as a case study because of the unmatched bonanza of cooperative phenomena appearing by changing the number n of perovskite layers. They range from high-temperature isotropic ferromagnetism in $SrRuO_3$ ($n = \infty$)[1] to anisotropic ferro- or meta-magnetic behavior of $Sr_4Ru_3O_{10}$ ($n = 3$), enhanced Pauli paramagnetism close to magnetic order in $Sr_3Ru_2O_7$ ($n = 2$)[2,3] and, finally, low-temperature superconductivity in Sr_2RuO_4 ($n = 1$).[4–7]

The amazing electronic properties of SRO perovskites are typically ascribed to two ingredients. The first is the interplay between lattice, spin, charge, and orbital degrees of freedom. This is, in principle, common to all transition-metal oxides (TMO). However, the radial extension of 4*d* atomic functions is significantly larger than that of 3*d* states. Hence in ruthenates the average electron-electron repulsion is weaker than in classical 3*d* TMOs, but the effects of structural distortions and bonding are more pronounced; at the same time, however, low-energy correlation effects are enhanced by Hund's rule coupling,[9] which results in large quasiparticle mass renormalizations of the electrons in the 4*d* t_{2g} bands.[10] Thus the ruthenates are materials in which a peculiar competition between local and itinerant physics takes place,[10,11] leading to quite different phenomena than in 3*d* TMOs. The second peculiar aspect is the layered structure (Fig. 1), believed to be by itself a source of intriguing phenomena. Following the experimental effort on other layered materials, such as cuprates,[12] cobaltates,[13] frustrated vanadates,[14] and Fe-based superconductors,[15,16] the study of ruthenium oxides has primarily focused on the role of the RuO_2 layers, which are believed to be mainly responsible for the emergent phenomena observed in these compounds. Several experimental works have been devoted to the study of the empty[8,17] and occupied[18] electronic states, mainly aiming to clarify the role played by the RuO_2 layers. Nevertheless, a complete picture of the electronic structure is still missing. In particular, the role of the SrO layers has been little investigated and the nature of the O bonds is not fully understood. This work aims to fill this gap.

To do this we use polarization-dependent resonant x-ray emission spectroscopy (XES).[19–21] Thanks to dipole selection rules and energy range analysis, resonant XES is an element and site-specific probe that provides access to the projection of occupied states onto inequivalent sites,[21–24] and thus to orbital occupations and anisotropies. To be able to clarify the nature of the oxygen bonds we perform measurements at the O *K* edge. This, in combination with *ab initio* calculations, allows us to separate the contributions of planar (O_p) and apical (O_a) oxygens, and ultimately to single out the RuO_2 and SrO layer contributions. Taken in conjunction with previous works, and in particular our x-ray absorption spectroscopy (XAS) results,[8] the present work establishes a complete picture of the electronic structure in the SRO family.

II. METHOD

A. Experiments

High quality $Sr_{n+1}Ru_nO_{3n+1}$ ($n = 1,2,3$) single crystals were fabricated by the flux-feeding floating zone technique, with Ru self-flux.[25–28] All sample surfaces were prepared *in situ* by cleaving in ultrahigh vacuum conditions.[8] The experimental work was carried out at the Beamline for Advanced diCHroism (BACH)[29,30] at Elettra. The O 1*s* XAS measurements were performed in the bulk sensitive fluorescence yield mode with an energy resolution of 0.15 eV. On- and off- resonance O *K*-edge XES measurements were acquired with a grating fluorescence spectrometer[31] and recorded in the second order of diffraction. For this set of measurements the combined resolving power Q of the beamline and the spectrometer monochromator was around 800 at the second diffraction order. The energy scale of the XES was calibrated

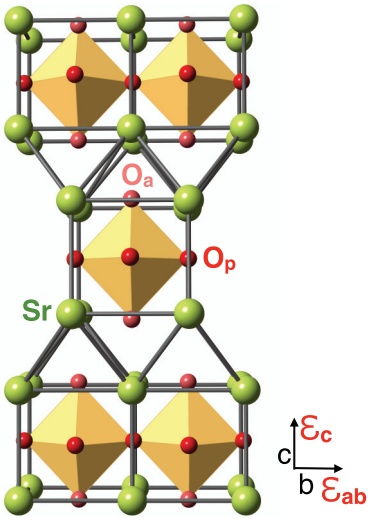

FIG. 1. (Color online) Crystal structure of the single-layered perovskite Sr_2RuO_4. Each Ru atom is surrounded by an octahedron constituted by six O atoms and by a cubic Sr cage. The c axis is perpendicular to the perovskite layers, and the ab plane is parallel to the plane formed by Ru atoms in a given perovskite layer.

using the Cu K-edge emission lines of pure copper metal. O $1s$ XAS and XES spectra for the three systems (Figs. 2 and 3) were acquired with fixed incident angle $\measuredangle(\hat{n},\hat{k}) = 60^\circ$, defined as the angle between the normal ($\hat{n}$) to the sample surface and the direction of the incoming beam $\hat{k}$. The photon polarization $\vec{\varepsilon}$ was varied from horizontal ($\vec{\varepsilon} \sim \vec{\varepsilon}_c$, i.e., almost parallel to c) to vertical ($\vec{\varepsilon} = \vec{\varepsilon}_{ab}$, i.e., parallel to the ab plane). The ab plane and c axis are specified in Fig. 1. This permits a precise study of the XAS/XES polarization dependence, without introducing geometrical factors due to different optical paths, and allows us to eliminate self-absorption effects. Due to the dipole selection rules, the in-plane field induces mainly O $1s \rightarrow$ O $2p_x$, O $2p_y$ excitations, while the out-of-plane $\vec{\varepsilon}$ induces exclusively O $1s \rightarrow$ O $2p_z$ transitions. Thus, by changing $\vec{\varepsilon}$ from horizontal to vertical states with different orbital symmetries are probed. The XES data are corrected for the energy-dependent incident photon flux and normalized to tabulated cross sections in an energy range about 40 eV above the O $1s$ threshold energy.

B. Theory

We assign the spectral features by comparison with *ab initio* calculations based on density-functional theory in the local-density approximation. We use two different first-principles approaches, both based on local orbitals. The first is the Nth-order linear muffin-tin orbital (NMTO) method and its Wannier functions, a powerful tool to disentangle the band structure and clarify the nature of bonding in complex transition-metal oxides.[32] The second is the linearized augmented plane-wave method (LAPW), which we use in the implementation of the WIEN2K package.[33] First we construct a complete set of NMTO Wannier functions and calculate the orbital-resolved hybridization matrices; next we combine these partial density of states to obtain the XES spectra, accounting for selection rules. We already successfully used such an approach to disentangle the various contributions to the XAS spectra in

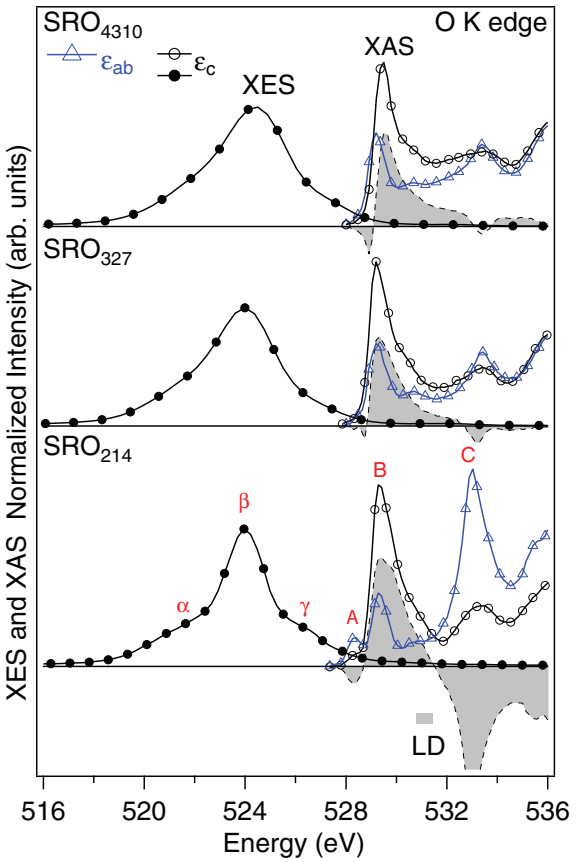

FIG. 2. (Color online) O K XES (circles) and XAS (triangles) spectra for the SRO series, measured at room temperature. The displayed XES spectra are recorded with excitation energy of 560 eV, well above the absorption threshold, i.e., off-resonance; at this energy the polarization dependence is basically negligible. The XAS spectra are shown for both polarization $\vec{\varepsilon}_c$ parallel to the c axis (horizontal, dark lines) and polarization $\vec{\varepsilon}_{ab}$ parallel to the the ab plane (vertical, light lines). For each system the linear dichroism $[\delta I_{\rm LD}(E) = I_{\rm XAS}(E;\vec{\varepsilon}_c) - I_{\rm XAS}(E;\vec{\varepsilon}_{ab})]$ is then shown (gray areas). The XAS data are from Ref. 8. All spectra are arranged together on a common energy axis.

Ref. 8. For horizontal polarization, the XES and XAS intensity can be estimated as $I(E;\vec{\varepsilon}_c) = \frac{1}{2}[\rho_x(E) + \rho_y(E)]\cos^2\theta_{\rm inc} + \rho_z(E)\sin^2\theta_{\rm inc}$, where $\theta_{\rm inc}$ is the incident angle, here fixed to 60°. The quantity $\rho_\alpha(E) = \sum_i \rho_{\alpha i}(E - \varepsilon_i^{1s})$ is the sum of orbital resolved oxygen density of states; $-\varepsilon_i^{1s}$ is the $1s$ core energy (with respect to the Fermi level) of the oxygen $i = {\rm O}_a, {\rm O}_p$ and $\alpha = x,y,z$. In the last step, we calculate the XES spectrum using the XSPEC program of the WIEN2K package; to directly compare with experimental spectra, we broaden the calculated spectra by a Gaussian function with 0.66 eV and full width at half maximum, with life-time broadening of the core state set to 0.64 eV.

III. RESULTS AND DISCUSSION

A. O *K* XAS and off-resonance XES

In Fig. 2 we show the XAS spectra, $I_{\rm XAS}(E;\vec{\varepsilon})$, together with XES spectra, $I_{\rm XES}(E;\vec{\varepsilon})$. The latter are normal or off-resonance, i.e., the data are taken at 560 eV, ~32 eV

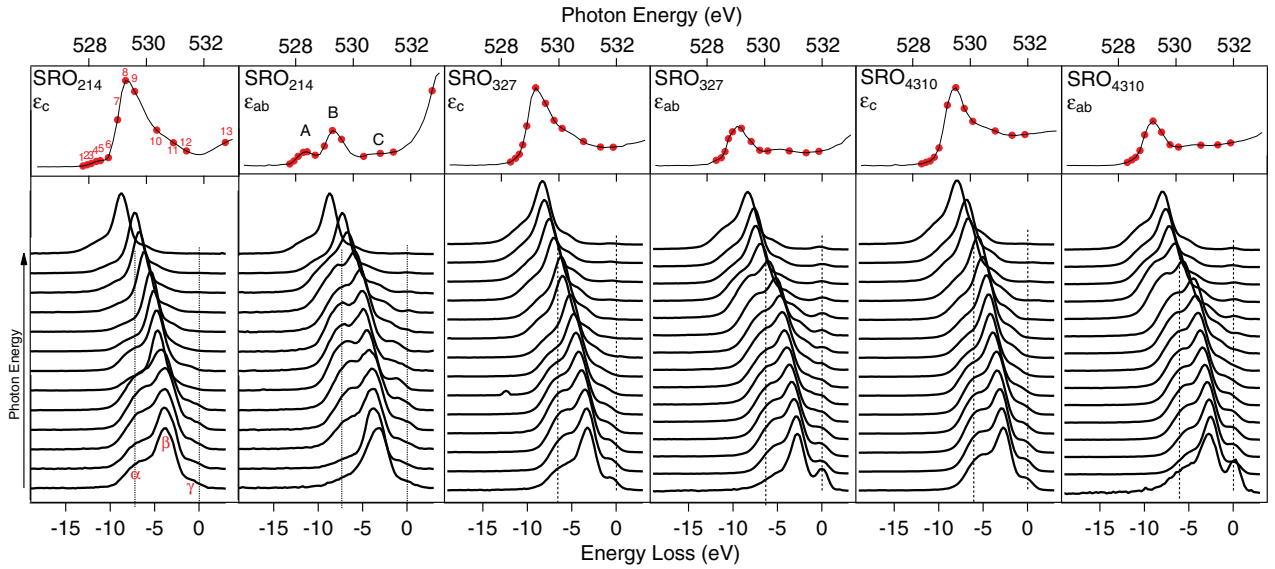

FIG. 3. (Color online) (Top row) O K-edge XAS of the SRO series ($n = 1,2,3$) for horizontal and vertical polarization, $\vec{\varepsilon}_c$ and $\vec{\varepsilon}_{ab}$. The numbered dots indicate the excitation photon energies at which the XES spectra (bottom row panels) are recorded. (Bottom row) O K-edge ($2p \rightarrow 1s$) XES spectra obtained at room temperature for several excitation energies and both horizontal and vertical polarization. For a given system and polarization the spectra are shifted vertically by a constant offset to the energy of incident exciting photons (numbered dots in the upper row panels). The spectra consist of elastically scattered light (the elastic peak, vertical dotted line) and an inelastic spectrum, composed by three main spectral features (α, β, and γ). The XES spectra are plotted vs the difference between the energy of the emitted and that of the incident photon (energy loss).

above the K-edge threshold. Since the x-ray absorption and emission spectra reflect the local density of empty and occupied electronic states, respectively, we combine the spectra in a plot with a common energy scale to facilitate the discussion. The energy calibration of the XAS and XES data was performed by comparison to the spectrum of a known reference sample. The spectra are shown for both horizontal $\vec{\varepsilon}_c$ and vertical polarization $\vec{\varepsilon}_{ab}$. All XAS spectra display a prominent feature B, with weaker shoulders A and C to its left and right, respectively. In Sr_2RuO_4 the A and B features form a double-peak structure which can be ascribed to the energy difference between apical and planar oxygen $1s$ core levels; such structure turns into a single peak with a tiny shoulder in $Sr_3Ru_2O_7$ and $Sr_4Ru_3O_{10}$. The nature of these XAS features has been discussed in previous works,[8,34,35] in particular Ref. 8. For clarity, here we briefly summarize our conclusions. Since the O $1s$ core-hole created during the XAS measurements weakly interacts with Ru $4d$ states, XAS data yield a relatively unperturbed probe of the Ru $4d$ DOS. The analysis of the Sr_2RuO_4 data shows that the pre-edge A feature mainly originates from the xz and yz bands, peak B from xy band, while peak C stems from Ru e_g holes. In the case of $n = 2$ and $n = 3$ compounds, due to the large spread in core-energy shifts, peak A splits and appears only as a shoulder of peak B. These assignments are supported by the difference $\delta I_{\rm LD}(E) = I_{\rm XAS}(E;\vec{\varepsilon}_c) - I_{\rm XAS}(E;\vec{\varepsilon}_{ab})$ yielding the out-of-plane/in-plane linear dichroism (LD), which turns out to be remarkably large. Finally, the change of the XAS and LD profiles in the different members of the SRO family reflects the structural changes in the unit cell with n, which results in a distinct rearrangement of the orbital occupation for the Ru t_{2g} and the O $2p$ bands.[8] Remarkably, we found that Sr d bands also sizably contribute, in particular to feature C, and are therefore essential to understand the XAS spectra.

Let us now turn to the off-resonance XES spectra in Fig. 2. For all the three compounds, the normal XES spectra are dominated by the strong central peak labeled with β and two weaker features labeled with α and γ. This spectral profile is consistent with previous experiments[36] on Sr_2RuO_4. At these energies the XES spectra display basically no polarization dependence. Finally, the spectral weight overlap of the low-energy loss feature γ and the lowest-energy peak A indicates the absence of an energy gap, and it is a direct evidence of the metallic nature of the three compounds. The nature of the α, β, and γ features is discussed in the next subsection, where we analyze the resonant XES spectra, i.e., those taken at or slightly above the energy of the K-edge threshold; in this energy regime the feature α is strongly enhanced.

B. Resonant XES

The resonant XES spectra are displayed in Fig. 3. The upper row panels show the XAS spectra in the photon energy range (526,533) eV for both horizontal and vertical polarization. The bottom row panels show the O $2p \rightarrow 1s$ XES spectra. The XES spectra are displayed as a function of the difference E between the energy of the incident and of the emitted photons, and hence the elastic peak is at zero energy. For a given system, the $I_{\rm XES}(E;\vec{\varepsilon})$ curves are displaced vertically by an amount proportional to the excitation energies. The latter are specified by the numbered dots superimposed to the XAS spectra in the corresponding upper panels, and vary from ~528 eV to ~533 eV. Particularly intriguing is the different effect of the polarization on the α and β features.

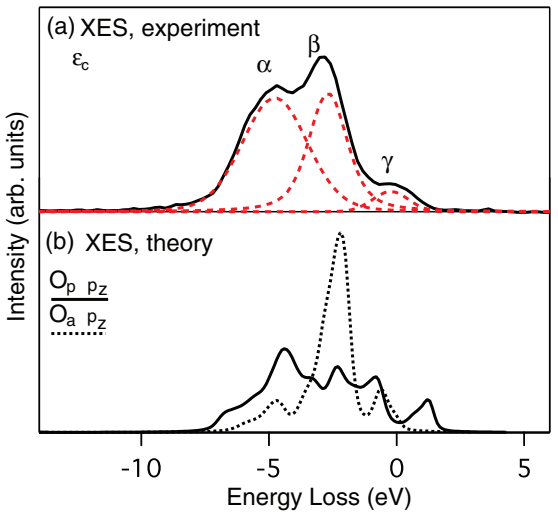

FIG. 4. (Color online) (a) XES O K-edge spectrum of Sr_2RuO_4 (black line) at the excitation energy 528.1 eV, horizontal polarization. The spectrum can be decomposed into three Lorentzian functions centered at -7, -4.6, and -1.3 eV, respectively (dashed lines). (b) Calculated O_a $2p_z$ (dotted line) and O_p $2p_z$ (solid line) contributions to the XES spectra in horizontal polarization, broadened by an instrumental resolution $\Delta E = 0.66$ eV.

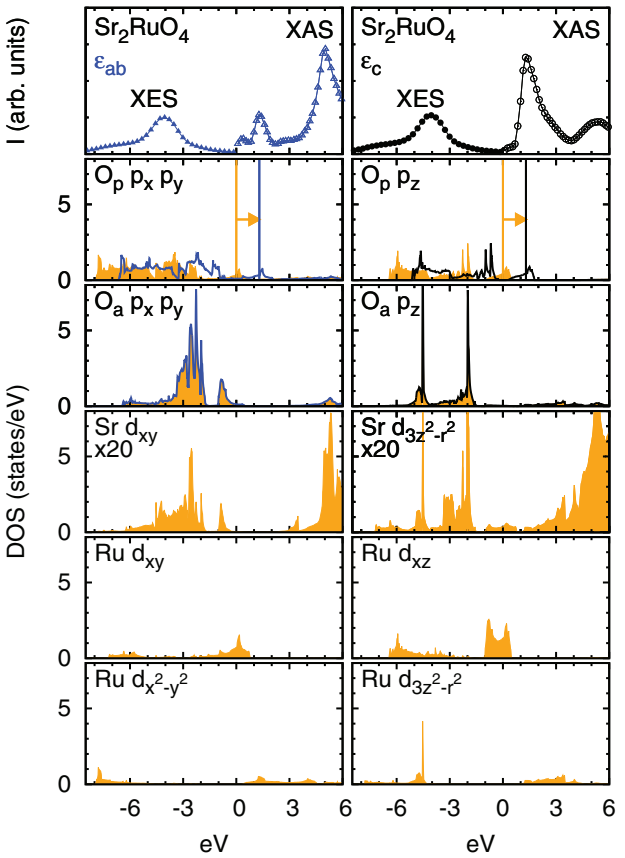

FIG. 5. (Color online) The two upper panels show the off-resonance XES and the XAS spectra for vertical (left column, triangles) and horizontal (right column, circles) polarization. The solid curves in the remaining panels show the most relevant partial density of states contributing to the spectra. The in-plane density of states are shown on the left and the out-of-plane density of states on the right. For the O_p $2p_x$, $2p_y$, and $2p_z$ contributions, the lines show the corresponding partial density of states shifted by $\sim$1.3 eV to account for the O 1s core-level energy difference between apical and planar oxygens. The shift is indicated by an arrow. The experimental data and the partial density of states are plotted on a common energy scale. For the experimental data we take as energy zero the absorption threshold, $E_0 \sim 528$ eV.

The main feature β, as well as the tiny feature γ, exhibit a nonresonant behavior in all the compounds, both for $\vec{\varepsilon}_c$ and $\vec{\varepsilon}_{ab}$ polarization and at all the excitation energies. The apparent small intensity variation of the γ feature around zero energy loss (low excitation energy) is caused by the overlap with the elastic peak. Through the XES profile simulations, shown in Fig. 4, we find that for horizontal polarization β has a major contribution from O_a p_z states; such contribution stems from the nonbonding bands hybridizing with Sr d states and centered at -2 eV, as evidenced by the Sr and O_a partial density of states displayed in Fig. 5. Thus, remarkably, peak β yields information on the evolution of the Sr-O_a hybridization in the SRO series.

The second feature α displays, differently from β and γ, a remarkable resonant behavior for both $\vec{\varepsilon}_c$ and $\vec{\varepsilon}_{ab}$ and in all systems. The evolution of α with the number of layers and with incident photon energy yields information on the Ru d-O p hybridization in the different materials and at different energies. Similar effects have been observed in previous works dealing with other highly anisotropic materials as NaV_2O_5.[37] We find that peak α has sizable contributions coming from the following hybridizations:

O_p $2p_z$-Ru $4d_{xz}$,
O_p $2p_x$, $2p_y$-Ru $4d_{xy}$, Ru $4d_{x^2-y^2}$,
O_a $2p_z$-Ru $4d_{z^2}$, Sr $3d_{3z^2-r^2}$,
O_a $2p_x$, $2p_y$-Ru $4d_{xz}$.

In order to single out which of these terms is important in which energy window we plot the maximum intensity of the spectral feature α as a function of the excitation photon energy and of the polarization direction. To this aim first we decompose the XES spectrum into a linear combination of three Lorentzian functions centered at -7, -4.6, and -1.3 eV, respectively. This decomposition is shown in Fig. 4(a). In Fig. 6 we show $R = I_\alpha/I_\beta$, the ratio between the maximum intensity of the resonant peak α and the intensity of the nonresonant peak β, which merely plays the role of normalization factor. We show R for both vertical and horizontal polarization, in all measured compounds and as a function of the excitation photon energies in the resonant energy ranges, defined in Table I. The I_α/I_β ratio exhibits a remarkable out-of-plane/in-plane anisotropy. For horizontal polarization $\vec{\varepsilon}_c$ (circles in Fig. 6) we find that $R = I_\alpha/I_\beta$ displays one relatively narrow peak centered at 528.1 eV for Sr_2RuO_4, and at 529.2 eV for $Sr_3Ru_2O_7$ and $Sr_4Ru_3O_{10}$. For planar polarization $\vec{\varepsilon}_{ab}$ (triangles in Fig. 6) we find instead that I_α/I_β displays a resonance spanning over a broader energy range. Interestingly, there is a partial overlap of the planar and vertical resonances. This happens at very low photon excitation energies. Finally, the energy widths ΔE of the resonant regimes (Table I) increases with the number of layers n, while an $\sim$0.6 eV energy shift of its onset is observed when passing from $n = 1$ to $n = 2,3$.

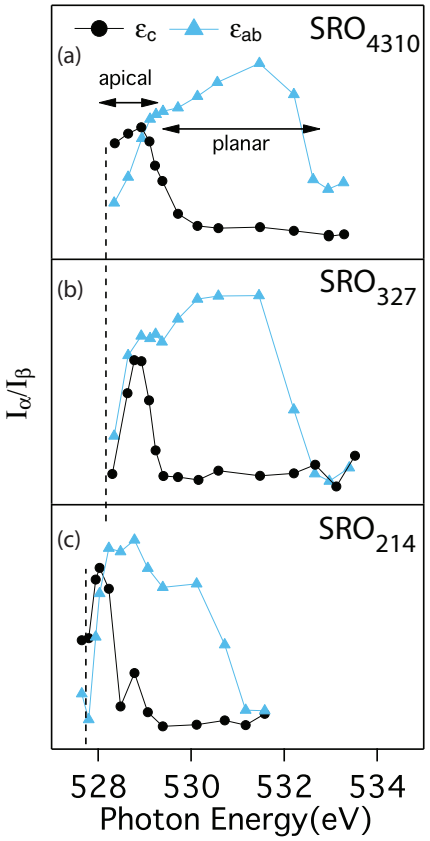

FIG. 6. (Color online) Intensity I_α of the resonant peak α normalized with respect to the intensity I_β of the nonresonant peak β as a function of the excitation photon energies. Black solid dots, $\vec{\varepsilon}_c$; solid triangles, $\vec{\varepsilon}_{ab}$. The arrows in panel (a) indicate the energy ranges of the $2p$ states of the apical and planar oxygens; the vertical dashed lines show the position of the elastic peak.

The striking polarization dependence of the resonance α can be rationalized by considering a poor man's one-electron picture of the XES mechanism. The photo-excited electron (spectator) is trapped into a bound, previously empty, orbital while an electron from an occupied state decays to fill the core hole. The lifetime of the photo-excited electron reflects the degree of localization of the excited bound state. Thus, the different resonant behavior displayed by our systems reflects the different in-plane and out-of-plane degrees of localization of the orbitals spanning the empty states.

Let us consider first the spectra for vertical polarization $\vec{\varepsilon}_{ab}$, which probe O_a and O_p p_x and p_y states. We find that the Ru d_{xz} and d_{yz} orbitals mostly hybridize with O_a p_x and p_y states

TABLE I. Energy range of the resonant intensity I_α for horizontal and vertical polarization and for all the samples. The energy difference ΔE is also reported. All energies are in eV.

	$\vec{\varepsilon}_c$		$\vec{\varepsilon}_{ab}$	
SRO	Energy range	ΔE	Energy range	ΔE
214	528.9–529.5	0.6	529–531.8	2.8
327	529.5–530.6	1.1	529.6–533.5	3.9
4310	529.5–531.4	1.9	530–534	4

while the Ru d_{xy} and $d_{x^2-y^2}$ orbitals hybridize, as expected, with O_p p_x and p_y (Fig. 6). Thus for vertical polarization $\vec{\varepsilon}_{ab}$ the ratio $R = I_\alpha/I_\beta$ reflects the width of the t_{2g} and e_g bands, sampled via the following hybridizations:

O_a p_x-Ru d_{xz},
O_a p_y-Ru d_{yz},
O_p p_x, p_y-Ru $d_{x^2-y^2}$,
O_p p_x, p_y-Ru d_{xy}.

The situation is very different for horizontal polarization $\vec{\varepsilon}_c$, i.e., when the O_a and O_p p_z states are sampled. For this polarization, the ratio $R = I_\alpha/I_\beta$ resonates in a small energy range above the Fermi level, and becomes tiny outside this energy region. For Sr_2RuO_4 the resonance is between 0 and 0.05 eV. In this energy window, because of the 1.3-eV shift towards higher energy of the planar O $1s$ core levels, there is no empty DOS from planar oxygens, as shown in Fig. 5. A similar shift of planar oxygen contributions to higher energy is also present in the $n = 2$ (∼1.6 eV) and $n = 3$ (∼0.05 eV) systems. Thus, at low energy, the ratio $R = I_\alpha/I_\beta$ measures O_a p_z holes. Our analysis shows that these holes are present in the low-energy t_{2g} bands via the small O_a p_z-Sr $d_{3z^2-r^2}$, Sr $d_{xz/yz}$ mixing. This conclusion is remarkable, since Sr states are typically neglected in the analysis of the low-energy electronic structure of the ruthenates and other layered materials. Our experiments can be seen as a direct confirmation of theoretical finding on the relevance of cation d states at low energy in the electronic structure of perovskites.[32] With respect to cubic perovskites,[32] in the layered ruthenates a further source of O_a p-Sr d mixing is the horizontal shifts of neighboring RuO_2 layers, which brings on top of each other Sr and O_a belonging to the surface of shifted perovskite layers (Fig. 1). In the case of Sr_2RuO_4, for Sr and O belonging to two neighboring Sr planes, the hopping integral between Sr $d_{3z^2-r^2}$ and O_c p_z is as large as 1.7 eV, and that between Sr d_{yz} and O_c p_y is ∼1.4 eV. The mixing of Sr d states in the t_{2g} bands can potentially have important consequences for the interpretation of experiments measuring the low-energy states of layered transition-metal perovskites. This assignment is confirmed by comparing the ratio R with the XAS linear dichroism shown in Fig. 2. The observed linear dichroism reflects the role played by apical and planar oxygen in different energy windows: the O_a contribution is the only one in the 0- to 0.5-eV energy range above the Fermi level, while the O_p orbital contribution is essential between 1 and 5 eV.[8]

IV. CONCLUDING REMARKS

In conclusion, by combining soft x-ray spectroscopic techniques and *ab initio* calculations, we have investigated the electronic structure of the $Sr_{n+1}Ru_nO_{3n+1}$ series ($n = 1,2,3$). By measuring the polarization resolved XAS and XES spectra at the O K edge on SRO single crystals, we have disentangled the contribution of the partial density of states of apical and planar oxygen p states. We have assigned all main features in the XES spectra. We have found that, surprisingly, Sr d states are very important to understand XES spectra, both below and above the Fermi level. Sr d orbitals participate in the low-energy electronic structure through the direct hybridization with the p orbitals of the apical oxygens.

ACKNOWLEDGMENTS

The authors are grateful to the staff of the BACH beamline and to Federico Salvador for technical support. The research leading to these results received funding from FP7/2007-2013 under Grant No. 264098-MAMA, as well as financial support from MIUR-PRIN 2008.

*marco.malvestuto@elettra.eu

[1] L. Klein, J. S. Dodge, C. H. Ahn, G. J. Snyder, T. H. Geballe, M. R. Beasley, and A. Kapitulnik, Phys. Rev. Lett. **77**, 2774 (1996).
[2] A. G. Green, S. A. Grigera, R. A. Borzi, A. P. Mackenzie, R. S. Perry, and B. D. Simons, Phys. Rev. Lett. **95**, 086402 (2005).
[3] A. Tamai, M. P. Allan, J. F. Mercure, W. Meevasana, R. Dunkel, D. H. Lu, R. S. Perry, A. P. Mackenzie, D. J. Singh, Z.-X. Shen, and F. Baumberger, Phys. Rev. Lett. **101**, 026407 (2008).
[4] J. Longo, P. Raccah, and J. Goodenough, J. Appl. Phys. **39**, 1327 (1968).
[5] Y. Maeno, H. Hashimoto, K. Yoshida, S. NishiZaki, T. Fujita, J. G. Bednorz, and F. Lichtenberg, Nature (London) **372**, 532 (1994).
[6] A. Mackenzie and Y. Maeno, Rev. Mod. Phys. **75**, 657 (2003).
[7] R. S. Perry, L. M. Galvin, S. A. Grigera, L. Capogna, A. J. Schofield, A. P. Mackenzie, M. Chiao, S. R. Julian, S. Ikeda, S. Nakatsuji, Y. Maeno, and C. Pfleiderer, Phys. Rev. Lett. **86**, 2661 (2001).
[8] M. Malvestuto, E. Carleschi, R. Fittipaldi, E. Gorelov, E. Pavarini, M. Cuoco, Y. Maeno, F. Parmigiani, and A. Vecchione, Phys. Rev. B **83**, 165121 (2011).
[9] L. de' Medici, J. Mravlje, and A. Georges, Phys. Rev. Lett. **107**, 256401 (2011).
[10] E. Gorelov, M. Karolak, T. O. Wehling, F. Lechermann, A. I. Lichtenstein, and E. Pavarini, Phys. Rev. Lett. **104**, 226401 (2010).
[11] E. Pavarini and I. I. Mazin, Phys. Rev. B **74**, 035115 (2006).
[12] A. Damascelli, Z. Hussain, and Z.-X. Shen, Rev. Mod. Phys. **75**, 473 (2003).
[13] E. Carleschi, M. Malvestuto, M. Zacchigna, A. Nicolaou, V. Brouet, S. Hébert, H. Muguerra, D. Grebille, and F. Parmigiani, Phys. Rev. B **80**, 035114 (2009).
[14] E. Pavarini, S. C. Tarantino, T. B. Ballaran, M. Zema, P. Ghigna, and P. Carretta, Phys. Rev. B **77**, 014425 (2008).
[15] H. Eschrig and K. Koepernik, Phys. Rev. B **80**, 104503 (2009).
[16] A. A. Kordyuk, Low Temp. Phys. **38**, 888 (2012).
[17] M. A. Hossain *et al.*, Phys. Rev. Lett. **101**, 016404 (2008).
[18] M. W. Haverkort, I. S. Elfimov, L. H. Tjeng, G. A. Sawatzky, and A. Damascelli, Phys. Rev. Lett. **101**, 026406 (2008).
[19] A. Kotani, Eur. Phys. J. B **47**, 3 (2005).
[20] C. Dallera and M. Grioni, Structural Chemistry **14**, 57 (2003).
[21] K. Okada and A. Kotani, J. Synchrotron Radiat. **8**, 243 (2001).
[22] A. Kotani and S. Shin, Rev. Mod. Phys. **73**, 203 (2001).
[23] A. Kotani, J. Electron Spectrosc. Relat. Phenom. **110**, 197 (2000).
[24] J. A. Carlisle, E. L. Shirley, L. J. Terminello, E. A. Hudson, J. J. Jia, T. A. Callcott, F. J. Himpsel, D. L. Ederer, and R. Perera, in *Materials Research Society Symposium–Proceedings* (Cambridge University Press, Cambridge, 1995), pp. 15–20.
[25] Z. Q. Mao, Y. Maeno, and H. Fukazawa, Mater. Res. Bull. **35**, 1813 (2000).
[26] R. Fittipaldi, D. Sisti, A. Vecchione, and S. Pace, Cryst. Growth Design **7**, 2495 (2007).
[27] R. Perry and Y. Maeno, J. Cryst. Growth **271**, 134 (2004).
[28] M. Zhou, J. Hooper, D. Fobes, Z. Mao, V. Golub, and C. Oconnor, Mater. Res. Bull. **40**, 942 (2005).
[29] M. Zangrando, M. Finazzi, G. Paolucci, G. Comelli, B. Diviacco, R. P. Walker, D. Cocco, and F. Parmigiani, Rev. Sci. Instrum. **72**, 1313 (2001).
[30] M. Zangrando, M. Zacchigna, M. Finazzi, D. Cocco, R. Rochow, and F. Parmigiani, Rev. Sci. Instrum. **75**, 31 (2004).
[31] D. Cocco, M. Matteucci, K. Prince, and M. Zangrando, Proc. SPIE-Int. Soc. Opt. Eng. **4506**, 46 (2001).
[32] E. Pavarini, A. Yamasaki, J. Nuss, and O. Andersen, New J. Phys. **7**, 188 (2005).
[33] P. Blaha, K. Schwarz, G. K. H. Madsen, D. Kvasnicka, and J. Luitz, *WIEN2K, An Augmented Plane Wave + Local Orbitals Program for Calculating Crystal Properties*, edited by K. Schwarz (Technische Universitat Wien, Austria, 2001).
[34] H.-J. Noh, S.-J. Oh, B.-G. Park, J.-H. Park, J.-Y. Kim, H.-D. Kim, T. Mizokawa, L. H. Tjeng, H.-J. Lin, C. T. Chen, S. Schuppler, S. Nakatsuji, H. Fukazawa, and Y. Maeno, Phys. Rev. B **72**, 052411 (2005).
[35] S. J. Moon, M. W. Kim, K. W. Kim, Y. S. Lee, J.-Y. Kim, J.-H. Park, B. J. Kim, S.-J. Oh, S. Nakatsuji, Y. Maeno, I. Nagai, S. I. Ikeda, G. Cao, and T. W. Noh, Phys. Rev. B **74**, 113104 (2006).
[36] E. Z. Kurmaev, S. Stadler, D. L. Ederer, Y. Harada, S. Shin, M. M. Grush, T. A. Callcott, R. C. C. Perera, D. A. Zatsepin, N. Ovechkina, M. Kasai, Y. Tokura, T. Takahashi, K. Chandrasekaran, R. Vijayaraghavan, and U. V. Varadaraju, Phys. Rev. B **57**, 1558 (1998).
[37] G. T. Woods, G. P. Zhang, T. A. Callcott, L. Lin, G. S. Chang, B. Sales, D. Mandrus, and J. He, Phys. Rev. B **65**, 165108 (2002).